A Phase-field Approach to Variational Hierarchical Surface Segmentation

Janos Meny, Martin Rumpf, Josua Sassen

Institute for Numerical Simulation, University of Bonn, Endenicher Allee 60, 53115 Bonn, Germany

Abstract

In this paper, we propose a phase-field model to partition a curved surface into path-connected segments with minimal boundary length. Phase-fields offer a powerful tool to represent diffuse interfaces with controlled width and to optimize them in a variational framework. We demonstrate how the multiplicative combination of phase-field functions can be used to effectively compute a hierarchical partition of unity. This induces an associated hierarchy of atlases, whose charts naturally overlap and thus are well-suited for applications such as texture mapping. Furthermore, we obtain distortion minimizing segmentations via a PDE-constraint optimization approach where the phase-field model allows direct use of Lagrangian calculus. Following Sharp and Crane (2018), the Yamabe equation, which allows computing the distortion induced by segment flattening, is considered as the constraint. This way, we obtain end-to-end diffuse formulations of variational problems in surface segmentation that are straightforward to treat computationally. Various examples illustrate the flexibility and robustness of this approach.

Keywords: phase-field model, shape optimization, topological constraints, hierarchical segmentation, atlas generation, yamabe equation

1. Introduction

Partitioning a surface into segments is a ubiquitous task in geometry processing. It is a core component in many algorithms that are used, for example, in computational design, remeshing, and texture mapping. These applications lead to different objectives for measuring the quality of a segmentation.

The application we consider in this paper is the generation of atlases, which is closely related to constructing surface parametrizations. The probably most famous example of this problem is to find an atlas of the earth, where different projections either have to distort the shape or size of landmasses. This example directly shows that there is not a single metric to determine what is a 'good' atlas. Typically different properties such as preserving angles, low area distortion, number of charts, and interface length need to be traded against each other. We can see an example of the trade-off between distortion and interface length in Figure 1. In computer graphics applications, conformal maps, i.e. preserving angles, have emerged as the dominating paradigm for generating charts. This raises the problem of constructing such conformal charts with minimal length and area distortion, which is typically approached by developing algorithms that try to optimally place the necessary cuts, i.e. dividers between segments, and is a very active area of research. In our work, we will take a slightly different approach and consider diffuse interfaces instead of sharp cuts.

Most existing algorithms focus on discrete cuts along the edges of a triangle mesh. However, optimal solutions might require cutting through triangles and thus some also consider such interfaces. A example for the latter is the work by Sharp and Crane (2018), who start from the continuous perspective and develop a PDE-constrained shape optimization of the distortion with the Yamabe equation as constraint. To this end, they construct a level set approach and this served as major inspiration for our work. However, level

Figure 1: Our approach produces segments with diffuse interfaces, shown here with a red to blue colormap, by solving a variational problem. By virtue of corresponding constraints, we can ensure that these segments are connected and cover the same amount of area. We can produce charts with overlapping support from these diffuse segments, shown are their images in the plane, and use them for mapping textures to the surface. However, when only using the perimeter as objective, as in the example on the left, the charts exhibit high distortion. Thus, we use the Yamabe equation for the logarithmic conformal factor as a PDE constraint and an objective involving this factor, which leads to distortion and perimeter minimizing segments as in the example on the right, where the textured hand is shown from two perspectives.

set approaches require careful handling of the interface in the optimization and are typically not well suited to deal with topology changes, e.g. promote them when desirable.

We also focus on the continuous perspective and develop a segmentation approach based on phase-fields. Phase-fields are a model for segments with diffuse interfaces that, in the case of two segments, assign each point on the surface a value between minus one and one. These endpoints figuratively correspond to two pure material phases while the range in between models a diffuse transition. Using phase-fields for computing surface segmentations yields a topologically flexible variational framework. This, however, could entail that our minimizers are disconnected and to mitigate this we employ the connectedness constraint introduced by Dondl et al. (2017). Furthermore, we introduce a novel hierarchical approach that multiplicatively combines multiple phase-fields to describe more than two segments. The resulting diffuse hierarchical segmentation can then be used to generate atlases with overlapping charts that are well-suited for applications such as texture mapping that we will show as a proof of concept. To control the distortion of these atlases, we introduce a diffuse version of the Yamabe equation that sidesteps any need to threshold the diffuse representation or explicitly cut the mesh. This end-to-end diffuse formulation of surface segmentation leads to variational problems that are straightforward to treat with conventional algorithms for nonlinear optimization.

Contributions. Our main contributions are:

- We provide a framework for using phase-fields to partition a curved surface into path-connected segments with minimal boundary length employing a connectedness constraint introduced by Dondl et al. (2017).

- We develop a novel hierarchical approach for surface segmentation based on multiple nested segments described via the multiplicative combination of phase-field functions.

- We show how to generate a corresponding hierarchy of atlases and an associated partition of unity, which are for instance useful for texture mapping as we demonstrate in a proof of concept.

- We pick up recent work by Sharp and Crane (2018) and consider a diffuse version of the Yamabe equation on phase-field described segments. We optimize these segments in a classical shape optimization approach with the Yamabe equation as a PDE constraint to minimize the conformal distortion when flattening the segments.

The combination of these contributions is, for example, demonstrated in Figure 1.

2

Organization. We begin in Section 2 by briefly discussing important previous work related to ours. Then we introduce our basic framework for segmenting the surface into two connected segments using phase-fields in Section 3. In Section 4, we introduce our hierarchical approach for computing multiple segments in a top-down fashion and discuss the application to atlas generation. Afterwards, in Section 5, we show how to minimize the distortion when flattening segments described by phase-fields. To this end, we introduce a diffuse version of the Yamabe equation and integrate this as a PDE constraint in the shape optimization problem for optimal segmentation. Finally, conclusions are drawn in Section 6.

2. Related Work

Many research questions touched in this paper, such as how to compute mesh segments for different tasks or how to place cuts on a surface such that it can be easily flattened have already be studied in recent publications.

Mesh Segmentation. Here, let us discuss a few examples that we deem particularly relevant with respect to our approach. A more extensive review of mesh segmentation approaches can, for example, be found in Shamir (2008).

Most approaches are concerned with discrete cuts, i.e. splitting or cutting the mesh along its edges. However, computing exact discrete minimizers for even basic taks such as finding the shortest cuts to obtain a topological disk (Erickson and Har-Peled, 2004) or a partition into equally-sized convex parts with minimal interface (Chazelle et al., 1997) are NP-hard. Hence, approximate solutions and algorithms to compute them are investigated.

With respect to atlas generation and related applications, curvature-based objectives have been used to compute segmentations. For example, Yamauchi et al. (2005) aim for an even distribution of Gauß curvature among the segments while Julius et al. (2005) determine how well conics fit the different segments. Both use their objectives as proxy for developability. In contrast, Lien and Amato (2007) compute decomposition into approximately convex parts by measuring the distance between them and their convex hull. This approach is speed-up by Mamou and Ghorbel (2009).

A very popular approach to the hierarchical segmentation of meshes was introduced by Garland et al. (2001), who hierarchically cluster the faces of a mesh by edge contractions in the dual graph using the planarity of resulting clusters as primary criterion. Attene et al. (2006) extend this via taking into account how well clusters are approximated by certain primitives (e.g. planes or cylinders). Furthermore, Katz and Tal (2003) use a probabilistic formulation and combine this with a top-down approach to recursive decomposition. Lai et al. (2006) also use such a top-down approach, but add semantic objectives based on the change in texture and use a Lloyd's-type clustering algorithm.

Cutting and Flattening. For problems such as texture mapping, parametrizations of the surface with low area distortion are of great interest. This motivates the study of algorithms to cut and flatten - i.e. parametrize - surfaces. In fact, many of the curvature-based segmentation methods listed above draw their inspiration from this problem. Zhou et al. (2004) used nonlinear dimensionality reduction methods based on spectral analysis as initialization for a nonlinear optimization of the charts. Other approaches focus on placing special vertices, e.g. cone singularities, and then connecting them with cuts. To reduce the distortion, some place them via a greedy ansatz (Springborn et al., 2008; Ben-Chen et al., 2008; Zhu et al., 2020). Others follow a global shape optimization technique (Soliman et al., 2018). Departing from greedy approaches and other heuristics, Poranne et al. (2017) and Li et al. (2019) compute patches that minimize the associated distortion. To this end, they explicitly compute the parametrization of different patches and simultaneously optimize their distortion and boundaries. Going further, Sharp and Crane (2018) use the Yamabe equation to compute the lowest possible distortion and thus circumvent the need to compute parametrizations during the optimization. To optimize over surface patches to be flattened, they use a level set approach to describe the shape of the patches and solve the shape optimization problem of minimal distortion. In particular, they allow cuts not aligned with triangle edges. To actually compute (approximately) conformal parametrizations of segments, an important approach was introduced by Lévy et al. (2002), who minimize a least-squares approximation of the associated Cauchy-Riemann equations.

Phase-fields on Surfaces. Phase-fields, or comparable diffuse interface models, on surfaces have already been used, for example, by Hornung et al. (2020) who use phase-fields to diffusely represent hard and soft material on the surface and optimize their distribution. Zayer et al. (2019) and Stadlbauer et al. (2020) use a diffuse representation to compute Voronoi-type diagrams by growing segments from a given start points. Even more general, Bertozzi and Flenner (2012) use diffuse interface models on arbitrary graphs and combine perimeter minimization with data-based fitting terms to address classification problems.

3. Phase-Field based Surface Segmentation

Let us begin with a presentation of the most important ingredients of our segmentation approach. To this end, assume $(\mathcal{M}, g)$ to be an orientable, two dimensional, compact Riemannian surface embedded in $\mathbb{R}^3$. Our first goal is to compute a segmentation $\mathcal{M} = \mathcal{M}^+ \cup \mathcal{M}^-$ with minimal length of the interface $\partial (\mathcal{M}^+ \cap \mathcal{M}^-)$ on $\mathcal{M}$ subject to the constraint that $\mathcal{M}^+$ and $\mathcal{M}^-$ have the same area. To define a suitable approximation of this segmentation problem, let us at first review a phase-field approach to describe interfacial energies and investigate the approximation of a connectedness constraint for the segments $\mathcal{M}^+$ and $\mathcal{M}^-$.

In this approach, the two segments will be described by a smooth function u which varies between -1 and 1 with a smooth and steep transition. Intuitively, one can think of this function describing the mixture of two materials on the surface where -1, 1 indicate the pure material phases. By postulating that these materials mix smoothly and have a desire to be as pure as possible, Modica and Mortola (Modica and Mortola, 1977) derived a functional $\mathcal{P}_\varepsilon[u]$ describing their behavior. Minimizers of this functional describe stable material distributions that consists of large pure phases and narrow transition zones between them. Here, ε describes a trade-off between smooth mixing and purity of phases that corresponds to the width of these transition zones. In fact, it turns out that the value of the Modica-Mortola functional approximates the length of the interface of the two segments and, when working on Euclidean domains, it is known to converge for decreasing interface width to the perimeter of a segment with sharp interfaces. This also justifies using phase-fields for the smooth approximation of segments on surfaces.

In what follows, we want to control and optimize multiple properties of segments described this way with the area being the easiest example. To describe these properties, we first introduce a smooth indicator function $\chi(u)$, which will be approximately 1 in the positive phase and drop to 0 when passing through the transition zone into the negative phase. By integrating this indicator function, we will obtain the approximate area $\mathcal{A}[u]$ of the positive phase. Furthermore, we want to ensure that our segments are connected. For this, we will use a functional $\mathcal{C}[u]$ adapting a corresponding functional for Euclidean domains Dondl et al. (2017) that essentially measures the lengths of shortest paths connecting different connected components of one phase and hence is zero when the phases are connected. These functionals will be discretized on a triangle mesh using affine finite elements.

For Euclidean domains, approaches based on phase-fields have been widely studied in the mathematical imaging community. Here, we will demonstrate that translating these approaches to surfaces is effortless and thus phase-fields can also be a powerful tool in geometry processing. In Section 4, we will consider the hierarchical segmentation of surfaces and, in Section 5, a diffuse approximation of the Yamabe equation for the conformal factor. Together, this can also be considered as a proof of concept for the use of phase-field models on surfaces.

Phase-fields on surfaces. We represent the segments using an approximating phase-field, i.e. via a phase-field function $u \colon \mathcal{M} \to \mathbb{R}$. This yields a convenient representation of the segments that allows for a simple approximation of the length of their interface by virtue of the Modica-Mortola functional (Modica and Mortola, 1977). Intuitively u describes two materials on the surface mixing at a diffuse interface layer. To this end, one considers a local chemical potential $\Psi \colon \mathbb{R} \to \mathbb{R}$ with two global minima at ± 1 representing the pure material phases $\mathcal{M}^+ = \{x \in \mathcal{M} : u \geq 0\}$ and $\mathcal{M}^- = \{x \in \mathcal{M} : u < 0\}$, respectively. The resulting total bulk energy of the phase-field is given by $\int_\mathcal{M} \Psi(u) \, \mathrm{d}\mathcal{H}^2$. To achieve smooth transitions between the phases, one adds an additional Dirichlet interface energy $\int_\mathcal{M} |\nabla u|^2 \, \mathrm{d}s$. With the proper scaling, we obtain the Modica-Mortola functional

$$\mathcal{P}_\varepsilon[u] = \int_\mathcal{M} \frac{\varepsilon}{2} |\nabla u|^2 + \frac{1}{\varepsilon} \Psi(u) \, \mathrm{d}\mathcal{H}^2, \tag{1}$$
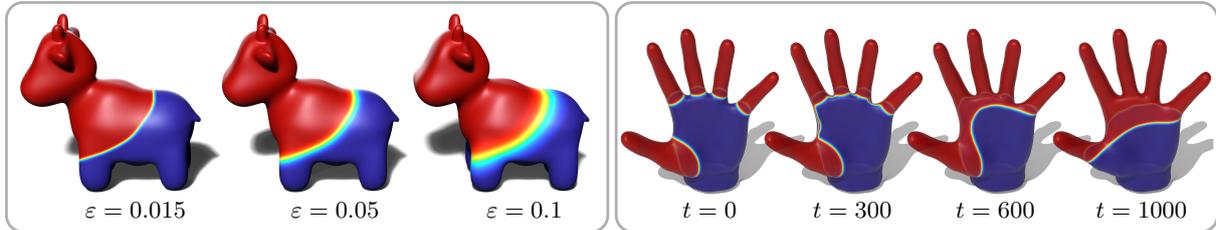
4

Figure 2: Results of the phase-field segmentation (6). Left: Interface minimization results for different values of ε yielding different interface widths. Right: Adding the connectedness constraint to the variational problem leads to a gradient descent flow (from which different time steps are shown) that connects phases while minimizing the interface perimeter.

where the parameter $\varepsilon > 0$ describes the width of the diffuse interface between the phases, as is shown in Figure 2 on the left. For $\varepsilon \to 0$, minimizing $\mathcal{P}_\varepsilon$ forces the phase-field towards the pure phases, and for a suitable choice of Ψ, the Modical-Mortola functional converges to the total interface length. More precisely, for $\Psi \in C^1(\mathbb{R})$ one obtains

$$\Gamma - \lim_{\varepsilon \to 0} \mathcal{P}_\varepsilon = c_\Psi \mathcal{P}$$

with respect to the $L^1(\mathcal{M})$-topology on Euclidean domains, where $c_\Psi = \int_{-1}^1 \sqrt{\Psi}\, d\mathcal{H}^2$, and, at least under smoothness requirements, this transfers to curved surfaces. Here $\mathcal{P}[u] := \mathcal{H}^1(\partial\{x \in \mathcal{M} : u(x) = 1\})$ if $u(\mathcal{M}) \subset \{-1, 1\}$ almost everywhere and $\mathcal{P}[u] := \infty$ else. In this case, ∂ denotes the measure-theoretic essential boundary.

The above result shows that for the particular choice $\Psi(u) = \frac{9}{16}(u^2 - 1)^2$, the constant c_Ψ is equal to one and the Modica-Mortola functional Γ-converges to the unscaled perimeter functional. From a practical point of view, this means that minimizers of the diffuse perimeter $\mathcal{P}_\varepsilon$ converge to minimizers of the regular perimeter for $\varepsilon \to 0$. Thus, it lends itself well as a functional representing the interface length of a phase-field described segmentation.

To define the area of the different phases, we need approximations of the indicator functions of the two phases. For this, we choose

$$\chi(u) := \frac{1}{4(1-\delta)^3}(u + 1 - \delta)^2(2(1-\delta) - u)$$

for $-1 + \delta \leq u \leq 1 - \delta$, $\chi(u) := 0$ for $u \leq -1 + \delta$, and $\chi(u) := 1$ for $u \geq 1 - \delta$ as a diffuse indicator for the positive phase $\mathcal{M}^+$. Here, δ is a small parameter with $0 < \delta \ll \varepsilon$. This way, $\chi \circ u$ ensures a localization of the transition region $\{x \in \mathcal{M} : \chi(u) \in (0, 1)\}$ taking into account that the optimal profiles for the phase-field u in (1) are of tanh-type (cf. (Modica and Mortola, 1977)). χ is C^1 smooth on $\mathbb{R}$, which is advantageous for the numerical minimization of functionals involving χ. Furthermore, the symmetry $\chi(-u) = 1 - \chi(u)$ ensures that $\chi(-u)$ is a proper approximation of a indicator function of the phase $\mathcal{M}^-$ and allows the definition of a partition of $\mathcal{M}$ based on χ. With χ at hand, the surface area of the phase $\mathcal{M}^+$ can be approximated via its integration, i.e

$$\mathcal{A}[u] := \int_{\mathcal{M}} \chi(u)\, d\mathcal{H}^2 \,, \tag{2}$$

where $\mathcal{A}[-u] = \mathcal{H}^2(\mathcal{M}) - \mathcal{A}[u]$.

Connectedness Constraint. Describing the segmentation using phase-fields offers a great deal of topological flexibility. However, in some of our targeted applications, we want to have some control over the topology of the segments. More concretely, the segmentation induced by a phase-field locally minimizing the Modica-Mortola functional might not be connected. To mitigate this, we pursue the method proposed by Dondl et al. (2017) for the Euclidean case. For a phase-field $u \in H^1(\mathcal{M})$, they suggest a method to enforce connectedness of the preimage $U = u^{-1}([\alpha, \beta])$ by introducing a differentiable penalty term. Let $F \in C^1(\mathbb{R})$ be a smooth function such that $F(u) = 0$ for all $u \in [\alpha, \beta]$ and $F > 0$ otherwise. Given two points $x, y \in U$, we can

5

define the weighted geodesic distance function $d^{F(u)}(x, y) = \inf \left\{ \int_\gamma F(u) \, \mathrm{d}\mathcal{H}^1 : \gamma \text{ curve from } x \text{ to } y \right\}$. This distance is zero for two points in the same connected component of U and positive for ones in different connected components. Hence, if u is continuous, then U is closed and $d^{F(u)}(x, y) = 0$ for all $x, y \in U$ if and only if U is path connected. From this follows that a quantitative measure for the path connectedness of U is given by $\int_{U \times U} d^{F(u)}(x, y) \, \mathrm{d}x \, \mathrm{d}y$. However, this depends on u in a non-differentiable fashion. This problem can be circumvented by introducing a smooth bump function $H \in \mathcal{C}^1(\mathbb{R})$ such that $H > 0$ on (α, β) and $H = 0$ on $\mathbb{R} \setminus (\alpha, \beta)$. Hence, one obtains the functional

$$\mathcal{C}[u] = \int_{\mathcal{M} \times \mathcal{M}} H(x) H(y) d^{F(u)}(x, y) \, \mathrm{d}x \, \mathrm{d}y, \tag{3}$$

which indeed is differentiable w.r.t. the phase-field parameter u.

In Figure 2, we see that combining the Modica-Mortola functional (1) and the connectedness term (3) in a variational problem leads to connected phases minimizing the interface perimeter. Indeed, Dondl et al. (2019) prove, in the Euclidean case, a Γ-convergence result for this combination to the usual perimeter functional $\mathcal{P}$ under a connectedness constraint in the sharp interface limit.

In detail, we choose the interval $[1 - \sqrt{\varepsilon}, 1]$ for the positive phase with corresponding functions

$$F(u) = \begin{cases} (u - 1 + \sqrt{\varepsilon})^2 & u \le 1 - \sqrt{\varepsilon} \\ 0 & u \ge 1 - \sqrt{\varepsilon} \end{cases}, \qquad H(u) = \begin{cases} 0 & u \le 1 - 2\sqrt{\varepsilon} \\ 1 & u \ge 1 - \sqrt{\varepsilon} \end{cases},$$

where H is smoothly interpolated between the given values using a cubic polynomial. For the negative phase, we mirror this at zero, i.e. we use $\mathcal{C}[-u]$.

Segmentation. Based on the phase-field approach and the corresponding connectedness constraint, we are in the position to formulate our basic segmentation problem. We ask for a solution of the following variational problem

$$\begin{aligned} \underset{u \in H^1(\mathcal{M})}{\text{minimize}} \quad & \mathcal{P}_\varepsilon[u] + \varepsilon^{-\kappa} \left(\mathcal{C}[u] + \mathcal{C}[-u] \right) \\ \text{subject to} \quad & \mathcal{A}[u] = \frac{1}{2} \mathcal{H}^2(\mathcal{M}), \end{aligned} \tag{4}$$

for $H^1(\mathcal{M})$ being the Sobolev space of functions with square integrable weak derivatives of order one on $\mathcal{M}$ and for some $\kappa > 0$ which is typically chosen to be one in experiments. Figure 2 shows solutions of this problem for two examples. If we do not require exactly matching areas but rather want to regularize our segmentation, then the area constraint $\mathcal{A}[u] = \frac{1}{2} \mathcal{H}^2(\mathcal{M})$ can also be relaxed using a properly scaled quadratic penalty $(\mathcal{A}[u] - \frac{1}{2} \mathcal{H}^2(\mathcal{M}))^2$. Furthermore, other constraints such as mechanical energies of the phases could be adapted from phase-fields on Euclidean domains or developed based on surface geometry and we only consider the area as a simple example for this.

Discretization. We employ simple affine finite elements to discretize problem (4). To this end, we will use a manifold triangle mesh $\mathcal{M}_h = (\mathcal{V}, \mathcal{E}, \mathcal{F})$ with vertices $\mathcal{V} \subset \mathbb{R}^3$, edges $\mathcal{E} \subset \mathcal{V} \times \mathcal{V}$, and faces $\mathcal{F} \subset \mathcal{V} \times \mathcal{V} \times \mathcal{V}$. Here, the subscript h indicates the grid size. Let us first recall the definition of the mass and stiffness matrix. Let $\theta_1, \ldots, \theta_{|\mathcal{V}|}$ be the nodal hat basis function and assume that the finite element approximation of u is in span of these functions with coefficient vector $\mathbf{u} \in \mathbb{R}^{|\mathcal{V}|}$. The double well potential of the phase-field $\Psi(u)$ is nonlinear and therefore not an element of the vector space spanned by the FEM basis functions, even if u is. Projecting it onto this vector space yields the coefficient vector $\Psi_h(\mathbf{u}) \in \mathbb{R}^{|\mathcal{V}|}$, $\Psi_h(\mathbf{u})_i = \Psi(\mathbf{u}_i)$, i.e. the piecewise linear interpolation of its nodal values.

The stiffness matrix $\mathbf{S} \in \mathbb{R}^{|\mathcal{V}| \times |\mathcal{V}|}$ is the discretization of the symmetric, positive definite quadratic form $\int_{\mathcal{M}} \nabla f \cdot \nabla g \, \mathrm{d}\mathcal{H}^2$ and thus its entries are given by $\mathbf{S}_{ij} := \int_{\mathcal{M}} \nabla \theta_i \cdot \nabla \theta_j \, \mathrm{d}\mathcal{H}^2$. This yields the well-known cotan entries (Dziuk, 1988). Hence, the Dirichlet energy of the phase-field u is discretized by $\mathbf{u}^T \mathbf{S} \mathbf{u}$. The mass matrix $\mathbf{M} \in \mathbb{R}^{|\mathcal{V}| \times |\mathcal{V}|}$ discretizes the quadratic form $\int_{\mathcal{M}} f g \, \mathrm{d}\mathcal{H}^2$. We choose a diagonal mass matrix, sometimes also called lumped mass matrix. The lumped masses $\mathbf{m} \in \mathbb{R}^{|\mathcal{V}|}$ are given by $\mathbf{m}_v = \frac{1}{3} \sum_{f \in \mathcal{F}: v \in f} \mathbf{a}_f$

with $\mathbf{a}_f$ being the area of the triangle f and the corresponding mass matrix is then the diagonal matrix $\mathbf{M} := \mathrm{diag}(\mathbf{m})$. Using the lumped mass matrix, the integral of $\Psi_h(\mathbf{u})$ over the surface of $\mathcal{M}_h$ can be approximated by a simple dot product $\mathbf{m}^T \Psi_h(\mathbf{u})$, yielding

$$\mathbf{P}_\varepsilon[\mathbf{u}] = \frac{\varepsilon}{2}\mathbf{u}^T\mathbf{S}\mathbf{u} + \frac{1}{\varepsilon}\mathbf{m}^T\Psi_h(\mathbf{w}) \tag{5}$$

as the discretization of (1). Similarly the quantity $\mathcal{A}(u)$ can be approximated by $\mathbf{m}^T\chi_h(\mathbf{u})$ with $\chi_h(\mathbf{u}) \in \mathbb{R}^{|\mathcal{V}|}$ defined via $\chi_h(\mathbf{u})_i = \chi(\mathbf{u}_i)$,

A convenient discretization of the connectedness constraint was introduced in Dondl and Wojtowytsch (2018), which is based on shortest-path searches in the dual graph of the triangle mesh. First, one computes for every triangle f the average u_f of the discrete phase-field u. Then every edge in the dual graph, i.e. every interior edge of the mesh, is equipped with a weight that is given by the product of the average value of $F(u_f)$ of the two adjacent triangles and the average of their diameters. This way distances on the dual graph approximate distances given by $d^{F(u)}$. Thus, to discretize the double integral $\mathcal{C}[u]$, components of the dual graph consisting of triangles with zero distance to each other are computed, as well as the distances and shortest paths between these components. Then the discretization $\mathbf{C}[\mathbf{u}]$ is given by the sum of pairwise products of integrated values of $H(u)$ for every pair of distinct components weighted by their distance. From this, also a discrete gradient can be computed, which is supported along the aforementioned shortest paths. For details on this discretization, we refer the reader to Dondl and Wojtowytsch (2018).

Overall, this leads to the finite-dimensional nonlinear optimization problem

$$\begin{aligned} &\underset{\mathbf{u} \in \mathbb{R}^{|\mathcal{V}|}}{\text{minimize}} && \mathbf{P}_\varepsilon[\mathbf{u}] + \varepsilon^{-\kappa}\left(\mathbf{C}[\mathbf{u}] + \mathbf{C}[-\mathbf{u}]\right) \\ &\text{subject to} && \mathbf{m}^T\chi_h(\mathbf{u}) = \frac{1}{2}\mathbf{a}. \end{aligned} \tag{6}$$

with the total surface area of $\mathcal{M}_h$ given by $\mathbf{a} = \mathrm{tr}\,\mathbf{M}$.

As (6) is a nonlinear optimization problem, we will compute local minimizers that depend on the initialization of $\mathbf{u}$. To this end, we opted for the simple approach of initializing with random values in $[-1, 1]$. However, to reduce the number of necessary iterations, one could also use fast heuristics, such as clustering of normal directions, or input from users to generate the initialization.

Implementation. We have implemented our method in C++ and provide the source code under `https://github.com/Janos95/Phasefields`. We use the Eigen library (Guennebaud et al., 2010) for numerical linear algebra and CHOLMOD (Chen et al., 2008) and UMFPACK (Davis, 2004) from the SuiteSparse collection as direct linear solvers. For unconstrained optimization problems, i.e. when using a quadratic penalty for the area constraint, we use libLBFGS, a limited memory BFGS implementation based on the work of Nocedal (1980). For constrained optimization problems, we use the open-source software package Ipopt (Wächter and Biegler, 2006) implementing an interior point method.

Phase-field Parameter. For the phase-fields, we have to choose the parameter ε governing the interface width. To achieve maximal detail, it should be chosen such that the interface covers two to three triangles in width. However, choosing ε too small can impede the numerical optimization, for example when it prevents the formation of paths connecting different components of a phase to fulfill the connectedness constraint. Hence, this is usually a difficult choice for strongly anisotropic meshes. To this end, we remeshed our examples isotropically using the method described by Botsch and Kobbelt (2004). This yields an approximately constant triangle diameter h and we can set $\varepsilon \approx 2h$. Wider interfaces are of course also possible, see e.g. Figure 5, and can facilitate the numerical optimization, which can be used to initialize computations with narrow interfaces.
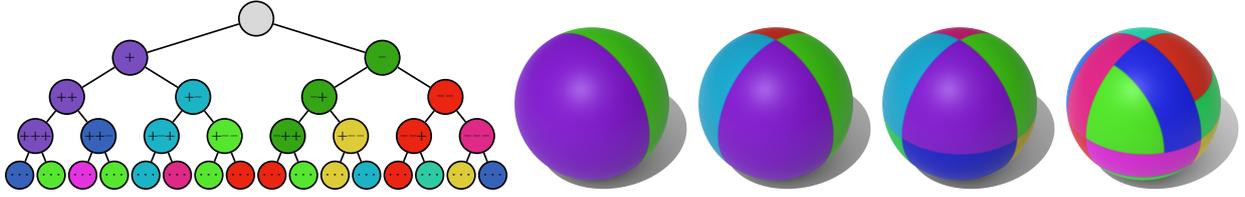
Figure 3: Hierarchical segmentation of the sphere: on the left the binary tree with nodes representing the $\alpha \in \{-1, +1\}^K$ with $K = 1, 2, 3$. The nodes are identically color coded as the corresponding segments on the right.

4. Hierarchical Segmentation

In this section, we will discuss a hierarchical generalization of the above segmentation approach. Thereby, we recursively perform a segmentation on previously already computed segments. To this end, we use additional phase-field functions for the next subdivision step and diffuse indicator functions identifying the segment to be further subdivided. Such a hierarchical segmentation is a flexible and useful tool. For example, with an increasing number of segments the geometric complexity of each segment decreases, which is advantageous for applications like fabrication. Furthermore, the segmentation hierarchy can be used for multi-resolution feature representations. For example, it can be used to generate the cluster tree for Tausch-White wavelets (Tausch and White, 2003) on triangle meshes, which require the segments to be connected and approximately equally sized to yield well-conditioned problems.

Phase-field model. To define a hierarchical segmentation, we construct a binary tree of labels as illustrated in Figure 3. Every node on level K of this tree represents a segment with diffuse indicator function χ^α with label $\alpha \in \{-1, +1\}^K$ describing the subsequent left-right choices in the tree. Hence, χ^α is recursively defined as the product of single level segmentation functions, i.e.

$$\chi^\alpha := \prod_{j=1}^{k} \chi(\alpha_j u^{\alpha^{j-}}),$$

where $\alpha^{j-} = (\alpha_1, \ldots, \alpha_{j-1})$ and $u^{\alpha_{j-}}$ is the single level phase-field function describing the segmentation of the sub domain with diffuse indicator function $\chi^{\alpha^{j-}}$. Hereby, $u = u^{\alpha_{1-}}$ denotes the phase-field for the initial segmentation of $\mathcal{M}$ as described in Section 3. The properties of χ ensure that $\{\chi^\alpha\}_{\alpha \in \{-1, +1\}^K}$ is a partition of unity on $\mathcal{M}$ for every K, i.e.

$$\sum_{\alpha \in \{-1, +1\}^K} \chi^\alpha(x) = 1$$

for all $x \in \mathcal{M}$.

The variational description of u^α is as follows. We consider a relaxed indicator function $\chi_\eta^\alpha = \chi^\alpha + \eta$ for $0 < \eta \ll 1$ and define a regularized diffuse interface length adapting the Modica-Mortola functional

$$\mathcal{P}_{\varepsilon, \eta, \alpha}[u] := \int_{\mathcal{M}} \frac{\varepsilon}{2} \chi_\eta^\alpha |\nabla u|^2 + \frac{1}{\varepsilon} \chi_\eta^\alpha \Psi(u) \, d\mathcal{H}^2 + \frac{1}{\sigma} \int_{\mathcal{M}} (1 - \chi^\alpha) u^2 \, d\mathcal{H}^2 \tag{7}$$

as well as a weighted approximate of the surface area functional

$$\mathcal{A}_\alpha[u] := \mathcal{A}[\chi^\alpha u] = \int_{\mathcal{M}} \chi^\alpha \chi(u) \, d\mathcal{H}^2.$$

8

Figure 4: Hierarchical segmentation on a torus. Left: the segmentation of a torus might quickly lead to disconnected local minima (top). Adding the connectedness constraint to the objective prevents this (bottom). Right: Different time steps of a gradient descent scheme for the variational problem (10) with connectedness constraint on level $K = 2$ and the segmentation of the associated left half of the torus starting from a random initialization.

Then, u^α is the solution of

$$
\begin{aligned}
&\underset{u \in H^1(\mathcal{M})}{\text{minimize}} && \mathcal{P}_{\varepsilon,\eta,\alpha}[u] \\
&\text{subject to} && \mathcal{A}_\alpha[u] = \frac{1}{2} \int_{\mathcal{M}} \chi^\alpha d\mathcal{H}^2.
\end{aligned}
\tag{8}
$$

As before in the single level segmentation problem, the constraint forces a splitting of the segment with indicator function χ^α into two equally sized segments with indicator functions $\chi^\alpha \chi(u)$ and $\chi^\alpha \chi(-u)$. The relaxation of χ^α in the definition of the diffuse perimeter functional $\mathcal{P}_{\varepsilon,\eta,\alpha}$ is required to ensure well-posedness of the above variational problem. In fact, u is still a function on the whole surface $\mathcal{M}$ and the first term of the perimeter functional is strictly coercive but the impact of values outside the current segment to be subdivided is strongly damped by η. Furthermore, the last term, with $0 < \sigma \ll 1$, acts as a penalty term forcing u to be close to zero outside the current segment.

This top-down approach allows to efficiently compute hierarchical segmentations where the interfaces between segments can flexible relax on each level of the hierarchy. However, this type of approach has the general limitation that the quality of lower level segmentations is limited by the already fixed higher level segmentations. In our experiments, we did not observe this to be a problem. However, our phase-field model would also allow to optimize all levels simultaneously by integrating the $\mathcal{P}_{\varepsilon,\eta,\alpha}$-terms into a single objective or by using methods from multi-objective optimization.

Discretization. Let $\mathbf{u} \in \mathbb{R}^{|\mathcal{V}|}$ be the FEM basis coefficients of the discrete counterpart of the phase-field u as before. To discretize the functionals defined above, we need to discretize the functions χ^α. Here, we simply approximate χ^α by a piecewise linear interpolation of its nodal values. To this end, we denote the vector of nodal values of χ^α by $\mathbf{w}^\alpha$, i.e. $\mathbf{w}_j^\alpha = \chi^\alpha(v_j)$ for $v_j \in V$. Furthermore, we use the componentwise product $\odot$ of vectors. Then, the discrete counterpart to the adapted Modica-Mortola functional from (7) is given by

$$
\mathbf{P}_{\varepsilon,\eta,\alpha}[\mathbf{u}] = \frac{\varepsilon}{2} \mathbf{u}^T \mathbf{S}^\alpha \mathbf{u} + \frac{1}{\varepsilon} \mathbf{m}^T (\mathbf{w}^\alpha \odot \Psi(\mathbf{u})) + \frac{1}{\sigma} \mathbf{m}^T ((\mathbf{1} - \mathbf{w}^\alpha) \odot \mathbf{u} \odot \mathbf{u}),
\tag{9}
$$

where $\mathbf{S}_{ij}^\alpha \coloneqq \int_{\mathcal{M}} \chi_\eta^\alpha \nabla\theta_i \cdot \nabla\theta_j \, d\mathcal{H}^2$, for which we use a simple midpoint quadrature to compute the entries, and $\mathbf{m}$ is the lumped masses as before. The discrete version of the hierarchical area functional is simply

given by $\mathbf{m}^T(\mathbf{w}^\alpha \odot \chi(\mathbf{u}))$. Thus, our discrete optimization problem becomes

$$
\begin{aligned}
&\underset{\mathbf{u} \in \mathbb{R}^{|\mathcal{V}|}}{\text{minimize}} \quad \mathbf{P}_{\varepsilon,\eta,\alpha}[\mathbf{u}] \\
&\text{subject to} \quad \mathbf{m}^T(\mathbf{w}^\alpha \odot \chi(\mathbf{u})) = \frac{1}{2}\mathbf{m}^T\mathbf{w}^\alpha.
\end{aligned}
\tag{10}
$$

In fact, in the spatially discrete model, the η-regularization of the perimeter functional turned out to be no longer necessary because of the regularizing effect of the finite element discretization. An example for this optimization can be seen in Figure 4.

Atlas Generation. To generate atlases from our hierarchical segmentation, we pick up the partition of unity $\{\chi^\alpha\}_{\alpha \in \{-1,+1\}^K}$ on level K of the hierarchy and consider $U^\alpha := \{x \in \mathcal{M} : \chi^\alpha(x) \neq 0\}$ as chart domains forming a cover of $\mathcal{M}$. To compute the actual chart maps $\varphi^\alpha : U^\alpha \to \mathbb{R}^2$, one can use any state-of-the-art algorithm, for which we chose LSCM (Lévy et al., 2002), while other, nonlinear algorithms such as CETM (Springborn et al., 2008) would also be possible. In Figure 5, atlases for different K are shown. Using the chart maps, any function f defined in $\mathbb{R}^2$ can be lifted to the surface by $f^\alpha := f \circ \varphi^\alpha$ to obtain multiple functions defined on the surface. These functions can then be smoothly blended via

$$
f^\mathcal{M} := \sum_\alpha \chi^\alpha f^\alpha
$$

using the χ^α as weighting functions. This blending and the underlying atlas can be useful for different applications requiring a domain decomposition, such as partition of unity methods for finite element simulations and ODE solvers on surfaces. The hierarchical nature of our segmentation could be used to devise multi-resolution approaches for these applications. As a simple proof of concept, here, we only demonstrate its use for an improved texture blending that can outperform conventional thresholding based approaches which segment the mesh into disjoint patches with sharp transitions between them. Concretely, we consider maps $f : \mathbb{R}^2 \to \mathbb{R}^c$ with $\mathbb{R}^c$ being some color space as demonstrated in Figure 5 (cf. Piponi and Borshukov (2000) for a similar seamless blending of textures on surfaces using subdivision methodology).

5. Distortion Optimal Segmentation

In this section, we will show how to reduce the distortion of chart mappings via an optimization of the underlying surface segmentation. To this end, we will first discuss the Yamabe equation on subsets U of $\mathcal{M}$ using a sharp interface formulation and then introduce a diffuse version based on our phase-field approach.

Yamabe Equation. Consider a flattening of an open set U of a surface $\mathcal{M}$, i.e. a differentiable map $\varphi : U \to \mathbb{R}^2$. It induces a new metric on U (differing from the metric due to the embedding) by $\tilde{g}_x(u,v) = d_x\varphi(u) \cdot d_x\varphi(v)$ and φ is called *conformal* if $\tilde{g} = e^{2s}g$ for some smooth function $s : U \to \mathbb{R}$ and the two metrics are called conformally equivalent. By the Riemann mapping theorem, such a conformal map exists for all U with disk-like topology. The conformal factor e^{2s} (or equivalently the log conformal factor s) quantifies the length and area distortion induced by φ.

As we want to optimize a segmentation of $\mathcal{M}$ that minimizes this distortion on the segments, let us recall next how to compute s without needing to explicitly compute φ. To this end, let $\nu : \mathcal{M} \to S^2$ be the outward pointing unit normal of $\mathcal{M}$, also known as Gauß map. The shape operator S is defined as the Jacobian of the Gauß map, i.e. for $x \in \mathcal{M}$, $S(x) := D\nu(x)$. The *Gauß curvature* is defined as $K = \kappa_1\kappa_2 = \det S$, where κ_1, κ_2 are the eigenvalues of S, called principal curvatures. A classical result (see e.g. Schoen and Yau (1994)) states that given a conformally equivalent metric $\tilde{g}$, the Gauß curvature $\tilde{K}$ induced by it is related to the original Gauß curvature via $e^{2s}\tilde{K} = K + \Delta_\mathcal{M}s$. From this Springborn et al. (2008) derived, that if $\tilde{g}$ is a flat ($\tilde{K} = 0$) conformally equivalent metric then its log conformal factor s minimizes the Dirichlet
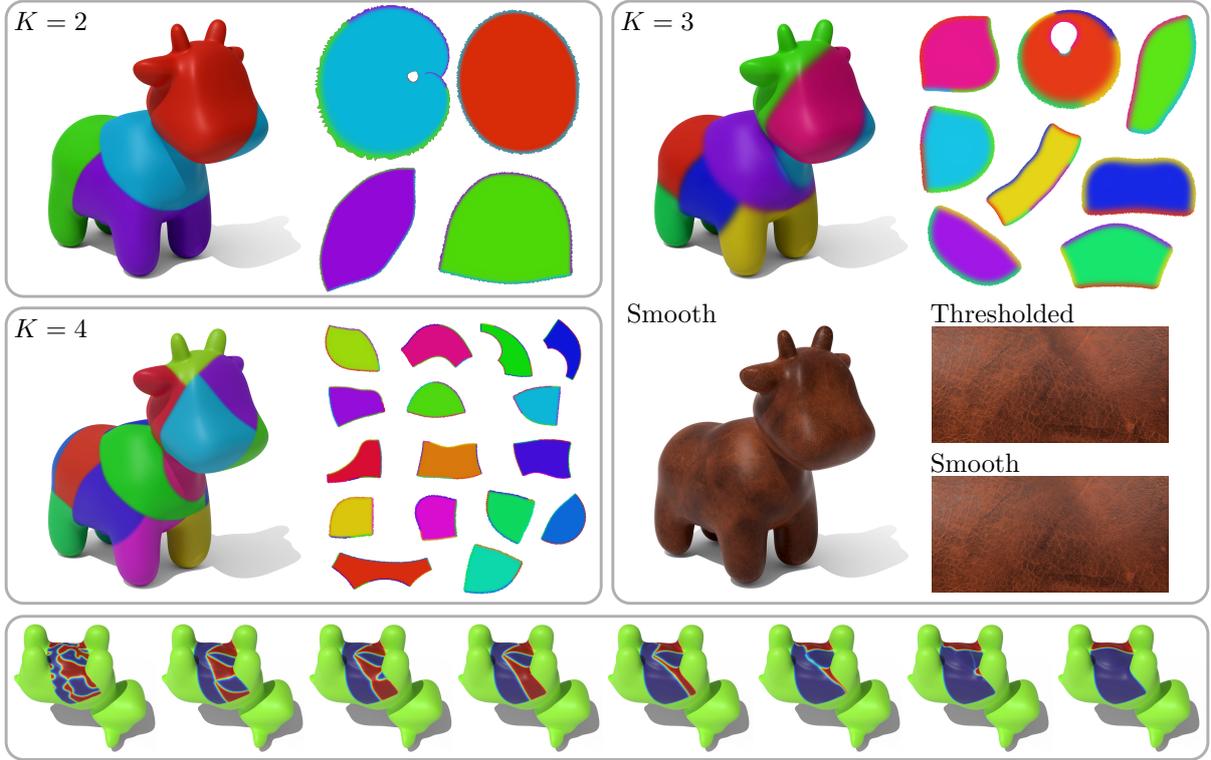
Figure 5: Hierarchical segmentation and atlas generation for $K = 2, 3$ and 4. The scalar functions χ^α are multiplied with different RGB color values identifying the different segments. Thereby, the diffuse glueing of the different chart domains is visible via the color blending close to the boundary of the chart domains U^α and their flattened counderparts $\varphi^\alpha(U^\alpha)$. On the lower right, texturing using the smooth phase-field based blending is compared with a conventional thresholding approach by zooming in on a textured surface. Note that, in the texturing application, we deliberately used a wider interface width ε to generate smoother transitions between the segments. On the bottom, we show different time steps of the descent scheme for one of the hierarchical segmentation steps on level $K = 4$.

energy among all flat conformal factors if s solves

$$
\begin{aligned}
\Delta_{\mathcal{M}} s &= -K, & U, \\
s &= 0, & \partial U,
\end{aligned}
\tag{11}
$$

where the boundary condition reflects the assumption that the metric does not change on the boundary. This PDE is also called the Yamabe equation (Aubin, 1998). The solution of this equation, in explicit its squared L^2-norm $\int_{\mathcal{M}} s^2 \, d\mathcal{H}^2$, called Hencky loss, is a measure of the required distortion to flatten the domain U. Hence, we will consider this equation as a constraint and minimize the sum of the squared L^2-norms of the solutions for the segmentation of $\mathcal{M}$.

Diffuse Yamabe Equation. To this end, we make use of the variational formulation of the Yamabe equation

$$
\min_{s \in H_0^1(U)} \int_U \frac{1}{2} |\nabla s|^2 - K s \, d\mathcal{H}^2.
$$

For u being a fixed phase-field segmentation of $\mathcal{M}$ as introduced in Section 3, we solve the Yamabe equation for both diffuse segments identified by $\chi(u)$ and $\chi(-u)$, respectively. In explicit, we seek functions $s = s[\pm u]$
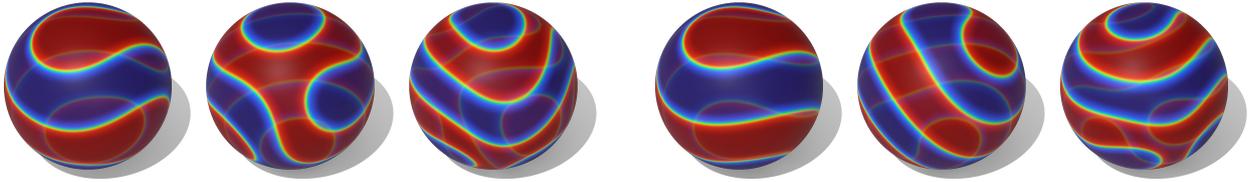
11

Figure 6: Solutions of (6) with distortion objective $\mathbf{J}^{\text{Yam}}$ on a sphere with approximately 40'000 vertices for different weights of the objective. The three spheres on the left show results without the connectedness constraint leading to disconnected phases with small 'islands', while the three spheres on the right show results using the connectedness constraint. In both cases, the interface parameter was $\varepsilon = 0.023$ and the weights were (from left to right) $\omega = 5, 10, 15$ respectively.

which minimize

$$\mathcal{Y}[u, s] = \int_{\mathcal{M}} \frac{1}{2}(\chi(u) + \eta)|\nabla s|^2 - \chi(u)sK + \frac{1}{\varepsilon} \cdot (1 - \chi(u))s^2 \, \mathrm{d}\mathcal{H}^2. \tag{12}$$

for given $\pm u$. Here, the factor $\chi(\pm u)$ localizes the minimization problem to one of the phases. The Dirichlet boundary condition is taken care of by a quadratic penalty term on the complementary phase forcing s to zero, which is akin to Nitsche's method for boundary conditions, and the η-damping ensures global regularity. The ε^{-1} scaling of the penalty in (12) ensures an increasing adherence of the boundary conditions for $\varepsilon \to \infty$.

The diffuse Yamabe equation is a quadratic problem in s, which means its solution can be computed by solving a linear problem. Furthermore, due to the uniform coercivity of the weighted Dirichlet energy and the smoothness of all coefficient functions $s[u]$ depends smoothly on u. Computing the Euler-Lagrange equation of (12), for fixed u, in direction $\theta \in H^1(\mathcal{M})$ yields

$$\partial_u \mathcal{Y}[u, s](\theta) = \int_{\mathcal{M}} \chi(u)\nabla s \cdot \nabla \theta - \chi(u)\theta K + \frac{1}{\varepsilon}(1 - \chi(u))s\theta \, \mathrm{d}\mathcal{H}^2.$$

Shape Optimization. Now, we define as already announced a new objective functional for our basic segmentation problem (4):

$$\mathcal{J}^{\text{Yam}}[u] = \int_{\mathcal{M}} s[u]^2 \, \mathrm{d}\mathcal{H}^2 + \int_{\mathcal{M}} s[-u]^2 \, \mathrm{d}\mathcal{H}^2,$$

where each of $s[\pm u]$ is the unique minimizer of (12) for the phase-fields $\pm u$. Finally, we are led to the PDE constrained optimization problem

$$
\begin{aligned}
\underset{u \in H^1(\mathcal{M})}{\text{minimize}} \quad & \mathcal{P}_\varepsilon[u] + \omega \mathcal{J}^{\text{Yam}}[u] + \varepsilon^{-\kappa} \left(\mathcal{C}[u] + \mathcal{C}[-u]\right) \\
\text{subject to} \quad & s[\pm u] \text{ minimizing } \mathcal{Y}[\pm u, \cdot], \text{ and} \\
& \mathcal{A}[u] = \frac{1}{2}\mathcal{H}^2(\mathcal{M}).
\end{aligned}
\tag{13}
$$

The factor ω controls the trade-off between interface length and distortion when flattening. Let us remark that the ε^{-1} scaling of the penalty in (12) appears to be the appropriate choice. In our experiments, we observed that for considering a penalty scaled with $\varepsilon^{-\beta}$ with $\beta > 1$ the distortion measure is reducing in a descent scheme at the expense of a growing perimeter of the interface between the segments. Figure 6 shows a comparison of distortion optimal segmentation without and with connectedness constraint.

Discretization and Implementation. We discretize the conformal factor via piecewise affine functions as we already did for phase-fields. Let $\mathbf{s} \in \mathbb{R}^{|\mathcal{V}|}$ denote the vector of coefficients w.r.t. to the nodal basis $\theta_1, \ldots, \theta_n$. Furthermore, we denote by $\mathbf{K} \in \mathbb{R}^{|\mathcal{V}|}$ the usual angle-defect discretization (see e.g. Cohen-Steiner and Morvan (2003)) of the Gauß curvature, i.e. $\mathbf{K}_i = \frac{1}{\mathbf{m}_i}(2\pi - \sum_{f: v_i \in f} \gamma_{f, v_i})$, where $\gamma_{f,v}$ is the interior angle in facet f at the vertex v. The discrete counter part of the diffuse Yamabe equation (12) is the linear system
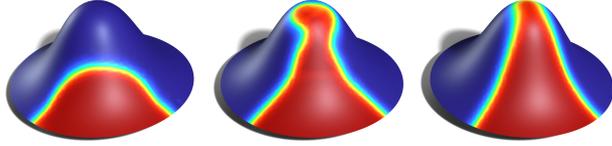
Figure 7: Three different time steps of the distortion minimization on a sinusoidal shaped surface. Interface width is given by $\varepsilon = 0.1$ and the distortion weight by $\omega = 10$. The result is similar to an analogous example by Sharp and Crane (2018).

$\mathbf{A}[u]\mathbf{s} = \mathbf{b}[u]$, where

$$\mathbf{A}[u] \coloneqq \mathbf{S}[u] + \frac{1}{\varepsilon}\mathrm{diag}((1 - \chi_h(\mathbf{u})) \odot \mathbf{m}), \qquad\qquad \mathbf{b}[u] \coloneqq \mathbf{m} \odot \chi_h(\mathbf{u}) \odot K,$$

with $\mathbf{S}_{ij}[u] \coloneqq \int_{\mathcal{M}}(\chi(u) + \eta)\nabla\theta_i \cdot \nabla\theta_j \, \mathrm{d}\mathcal{H}^2$. The discrete counterpart of $\mathbf{J}^{\text{Yam}}$ is given by

$$\mathbf{J}^{\text{Yam}}[\mathbf{u}] = \mathbf{s}[\mathbf{u}]^T\mathbf{M}\mathbf{s}[\mathbf{u}] + \mathbf{s}[-\mathbf{u}]^T\mathbf{M}\mathbf{s}[-\mathbf{u}].$$

To minimize the objective $\mathbf{J}^{\text{Yam}}[\mathbf{u}]$, we need to compute in particular its derivatives. Here, we follow the general procedure of shape optimization calculus. Recall, that we have $\mathbf{s}[\mathbf{u}] = \mathbf{A}[\mathbf{u}]^{-1}\mathbf{b}[\mathbf{u}]$, which implies that the first variation is given by

$$\partial_{\mathbf{u}}\mathbf{s}[\mathbf{u}] = \mathbf{A}[\mathbf{u}]^{-1}\left(\partial_{\mathbf{u}}\mathbf{b}[\mathbf{u}] - \partial_{\mathbf{u}}\mathbf{A}[\mathbf{u}]\,\mathbf{s}[\mathbf{u}]\right).$$

By applying the chain rule and using that $\mathbf{A}[\mathbf{u}]$ is symmetric, we obtain

$$\begin{aligned}\partial_{\mathbf{u}}\mathbf{J}^{\text{Yam}}[\mathbf{u}] = &- 2\left(\partial_{\mathbf{u}}\mathbf{b}[\mathbf{u}] - \partial_{\mathbf{u}}\mathbf{A}[\mathbf{u}]\,\mathbf{s}[\mathbf{u}]\right)^T \mathbf{A}[\mathbf{u}]^{-1}\left(\mathbf{M}\mathbf{s}[\mathbf{u}]\right) \\ &- 2\left(\partial_{\mathbf{u}}\mathbf{b}[-\mathbf{u}] - \partial_{\mathbf{u}}\mathbf{A}[-\mathbf{u}]\,\mathbf{s}[-\mathbf{u}]\right)^T \mathbf{A}[-\mathbf{u}]^{-1}\left(\mathbf{M}\mathbf{s}[-\mathbf{u}]\right).\end{aligned}$$

Hence, computing the derivative mainly amounts to solving two linear systems, where the matrices are the same as for the diffuse scale factors. If we use direct solvers such as a Cholesky decomposition, we can reuse the factorization and only have to compute additional back substitutions. In Figure 6, the effect of the factor ω is shown when segmenting a sphere. Depending on the application, one can also only use parts of (13). For example, in Figure 7, we show steps of a gradient-based flow for the problem without the area constraint. Following the approach described in Section 4, distortion aware hierarchical segmentation is also possible. Furthermore, in Figures 1 and 8 the quality of the distortion optimized segmentations is showing close to conformal texture transfer from associated chart domains onto the surface $\mathcal{M}$. In Figure 9, we see another example of a distortion minimizing segmentation for a more complex surface, which ´yields segment boundaries along paths with negative Gauß curvature in this example.

6. Conclusion

We introduced a framework for the numerical segmentation of surfaces using phase-fields as diffuse description of segments. In the description, we started with a basic optimization problem for segmenting a surface into two connected components of equal area that combines the Modica-Mortola perimeter approximation, the connectedness constraint from Dondl et al. (2017), and an area constraint. Generalizing this, we introduced a hierarchical approach based on the multiplicative combination of diffuse indicator functions that enables a flexible and nested segmentation of surfaces. Furthermore, we pick up the work of Sharp and Crane (2018) by introducing a diffuse version of the Yamabe equation that can be directly incorporated into our phase-field optimization to compute segments that can be conformally flattened with low area distortions. One common application of such segmentations is the generation of surface atlases with controlled overlap of the chart domains on the surface. These atlases can have various applications
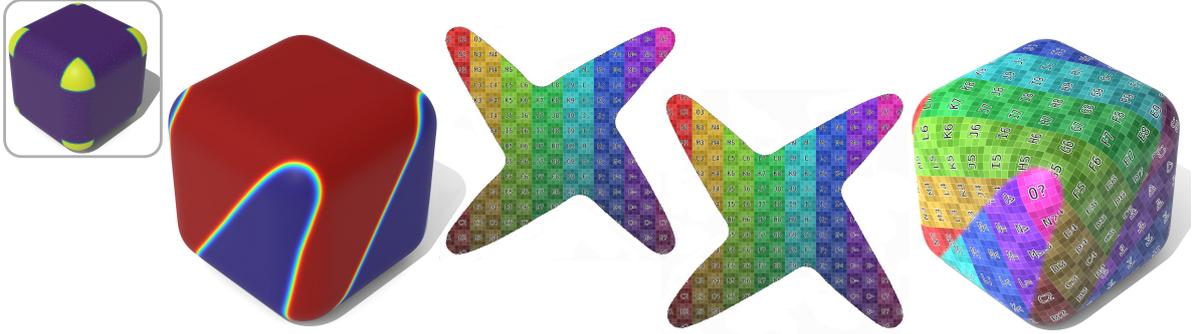
Figure 8: Segmenting and flattening a cube with rounded corners. The cube exhibits isolated regions of Gauß curvature at its rounded corners, which leads to a segmentation with boundaries not following the edges of the cube. Instead, the boundaries are such that their length in the isolated region is maximized while keeping the total length under control. From left to right: The discrete Gauß curvature shown as color map with dark blue indicating approximately zero curvature and yellow approximately 3.12 curvature. Solutions of (6) with distortion objective $\mathbf{J}^{\text{Yam}}$ and distortion weight $\omega = 10$. Conformally flattened segments in the plane with texture applied. Textures mapped to rounded cube, where perpendicular lines show the conformality and equally sized squares show the low distortion of the charts.

Figure 9: Distortion minimizing segmentation of the 'fertility' model (courtesy of the AIM@SHAPE project). Interface width is given by $\varepsilon = 0.02$ and the distortion weight by $\omega = 0.1$. For this example, minimizing (13) yields segment boundaries following paths with negative Gauß curvature.

and, as one example, we demonstrated that this approach is particularly suitable for seamlessly combing unstructured textures.

Limitations and Future Work. There are many ways how our method could be extended. Its main drawback so far is that we need high-resolution meshes for narrow diffuse interfaces and larger weights of the distortion objective. This leads to significant computational costs in these cases and, furthermore, generating the mesh requires access to an underlying smooth surface. To address the costs, adaptive refinement and multi-resolution approaches might be suitable options while intrinsic triangulations (Bobenko and Springborn, 2007) could enable the description of narrow transitions already on coarse meshes. Moreover, they could also allow to generate refined, isotropic meshes while preserving the extrinsic geometry of the mesh. Theoretical investigations such as the study of existence, uniqueness, and convergence of minimizers of the diffuse Yamabe equation as well as of the ensuing shape optimization problem are still open. This analysis could also help to better understand the appropriate scaling of the different terms in the context of refinement. Furthermore, our approach allows to ensure the connectivity of the segments. However, for many applications, it would be interesting to even guarantee simply-connectedness via a corresponding diffuse constraint, e.g. to ensure the existence of conformal charts. Lastly, we believe that our framework is also interesting for other mesh segmentation tasks by using other objectives, e.g. promoting normal consistency or convexity of segments.

14

Acknowledgments

References

Attene, M., Falcidieno, B., Spagnuolo, M., 2006. Hierarchical mesh segmentation based on fitting primitives. The Visual Computer 22, 181–193. doi:10.1007/s00371-006-0375-x.

Aubin, T., 1998. Some Nonlinear Problems in Riemannian Geometry. Springer Monographs in Mathematics, Springer Berlin Heidelberg, Berlin, Heidelberg. doi:10.1007/978-3-662-13006-3.

Ben-Chen, M., Gotsman, C., Bunin, G., 2008. Conformal Flattening by Curvature Prescription and Metric Scaling. Computer Graphics Forum 27, 449–458. doi:10.1111/j.1467-8659.2008.01142.x.

Bertozzi, A.L., Flenner, A., 2012. Diffuse Interface Models on Graphs for Classification of High Dimensional Data. Multiscale Modeling & Simulation 10, 1090–1118. doi:10.1137/11083109X.

Bobenko, A.I., Springborn, B.A., 2007. A Discrete Laplace–Beltrami Operator for Simplicial Surfaces. Discrete & Computational Geometry 38, 740–756. doi:10.1007/s00454-007-9006-1.

Botsch, M., Kobbelt, L., 2004. A remeshing approach to multiresolution modeling, in: Proceedings of the 2004 Eurographics/ACM SIGGRAPH symposium on Geometry processing, ACM Press, New York, New York, USA. p. 185. doi:10.1145/1057432.1057457.

Chazelle, B., Dobkin, D.P., Shouraboura, N., Tal, A., 1997. Strategies for polyhedral surface decomposition: An experimental study. Computational Geometry: Theory and Applications 7, 327–342. doi:10.1016/S0925-7721(96)00024-7.

Chen, Y., Davis, T.A., Hager, W.W., Rajamanickam, S., 2008. Algorithm 887: CHOLMOD, Supernodal Sparse Cholesky Factorization and Update/Downdate. ACM Transactions on Mathematical Software 35, 22:1–22:14. doi:10.1145/1391989.1391995.

Cohen-Steiner, D., Morvan, J.M., 2003. Restricted delaunay triangulations and normal cycle, in: Proceedings of the nineteenth conference on Computational geometry - SCG '03, ACM Press, New York, New York, USA. p. 312. doi:10.1145/777792.777839.

Davis, T.A., 2004. Algorithm 832: UMFPACK V4.3—an Unsymmetric-pattern Multifrontal Method. ACM Transactions on Mathematical Software 30, 196–199. doi:10.1145/992200.992206.

Dondl, P., Wojtowytsch, S., 2018. Keeping it together: a phase field version of path-connectedness and its implementation arXiv:1806.04767.

Dondl, P.W., Lemenant, A., Wojtowytsch, S., 2017. Phase Field Models for Thin Elastic Structures with Topological Constraint. Archive for Rational Mechanics and Analysis 223, 693–736. doi:10.1007/s00205-016-1043-6.

Dondl, P.W., Novaga, M., Wirth, B., Wojtowytsch, S., 2019. A Phase-field Approximation of the Perimeter under a Connectedness Constraint. SIAM Journal on Mathematical Analysis 51, 3902–3920. doi:10.1137/18M1225197.

Dziuk, G., 1988. Finite elements for the Beltrami operator on arbitrary surfaces, in: Hildebrandt, S., Leis, R. (Eds.), Partial Differential Equations and Calculus of Variations. Springer, Berlin. volume 1357 of *Lecture Notes in Math.*, pp. 142–155.

Erickson, J., Har-Peled, S., 2004. Optimally Cutting a Surface into a Disk. Discrete and Computational Geometry 31, 37–59. doi:10.1007/s00454-003-2948-z.

Garland, M., Willmott, A., Heckbert, P.S., 2001. Hierarchical face clustering on polygonal surfaces, in: Proceedings of the 2001 Symposium on Interactive 3D graphics - SI3D '01, ACM Press, New York, New York, USA. pp. 49–58. doi:10.1145/364338.364345.

Guennebaud, G., Jacob, B., Others, 2010. Eigen v3. http://eigen.tuxfamily.org.

Hornung, P., Rumpf, M., Simon, S., 2020. On Material Optimisation for Nonlinearly Elastic Plates and Shells. arXiv:2002.12615.

Julius, D., Kraevoy, V., Sheffer, A., 2005. D-Charts: Quasi-Developable Mesh Segmentation, in: Computer Graphics Forum, Citeseer. pp. 581–590. doi:10.1111/j.1467-8659.2005.00883.x.

Katz, S., Tal, A., 2003. Hierarchical mesh decomposition using fuzzy clustering and cuts. ACM Transactions on Graphics 22, 954–961. doi:10.1145/882262.882369.

Lai, Y.K., Zhou, Q.Y., Hu, S.M., Martin, R.R., 2006. Feature sensitive mesh segmentation, in: Proceedings of the 2006 ACM symposium on Solid and physical modeling - SPM '06, ACM Press, New York, New York, USA. p. 17. doi:10.1145/1128888.1128891.

Lévy, B., Petitjean, S., Ray, N., Maillot, J., 2002. Least squares conformal maps for automatic texture atlas generation. ACM Transactions on Graphics 21, 362–371. doi:10.1145/566654.566590.

Li, M., Kaufman, D.M., Kim, V.G., Solomon, J., Sheffer, A., 2019. OptCuts: Joint Optimization of Surface Cuts and Parameterization. ACM Transactions on Graphics 37, 1–13. doi:10.1145/3272127.3275042.

Lien, J.M., Amato, N.M., 2007. Approximate convex decomposition of polyhedra, in: Proceedings of the 2007 ACM symposium on Solid and physical modeling - SPM '07, ACM Press, New York, New York, USA. p. 121. doi:10.1145/1236246.1236265.

Mamou, K., Ghorbel, F., 2009. A simple and efficient approach for 3D mesh approximate convex decomposition, in: 2009 16th IEEE International Conference on Image Processing (ICIP), IEEE. pp. 3501–3504. doi:10.1109/ICIP.2009.5414068.

Modica, L., Mortola, S., 1977. Un esempio di Γ^--convergenza. Boll. Un. Mat. Ital. B (5) 14, 285–299.

Nocedal, J., 1980. Updating Quasi-Newton Matrices with Limited Storage. Mathematics of Computation 35, 773. doi:10.2307/2006193.

Piponi, D., Borshukov, G., 2000. Seamless texture mapping of subdivision surfaces by model pelting and texture blending, in: Proceedings of the 27th annual conference on Computer graphics and interactive techniques - SIGGRAPH '00, ACM Press, New York, New York, USA. pp. 471–478. doi:10.1145/344779.344990.

Poranne, R., Tarini, M., Huber, S., Panozzo, D., Sorkine-Hornung, O., 2017. Autocuts: simultaneous distortion and cut optimization for UV mapping. ACM Transactions on Graphics 36, 1–11. doi:10.1145/3130800.3130845.

Schoen, R.M., Yau, S.T., 1994. Lectures on differential geometry. Cambridge, MA : International Press.

Shamir, A., 2008. A survey on Mesh Segmentation Techniques. Computer Graphics Forum 27, 1539–1556. doi:10.1111/j.1467-8659.2007.01103.x.

Sharp, N., Crane, K., 2018. Variational surface cutting. ACM Transactions on Graphics 37, 1–13. doi:10.1145/3197517.3201356.

Soliman, Y., Slepčev, D., Crane, K., 2018. Optimal cone singularities for conformal flattening. ACM Transactions on Graphics 37, 1–17. doi:10.1145/3197517.3201367.

Springborn, B., Schröder, P., Pinkall, U., 2008. Conformal equivalence of triangle meshes. ACM Transactions on Graphics 27, 1–11. doi:10.1145/1360612.1360676.

Stadlbauer, P., Mlakar, D., Seidel, H.P., Steinberger, M., Zayer, R., 2020. Interactive Modeling of Cellular Structures on Surfaces with Application to Additive Manufacturing. Computer Graphics Forum 39, 277–289. doi:10.1111/cgf.13929.

Tausch, J., White, J., 2003. Multiscale bases for the sparse representation of boundary integral operators on complex geometry. SIAM Journal on Scientific Computing 24, 1610–1629. doi:10.1137/S1064827500369451.

Wächter, A., Biegler, L.T., 2006. On the implementation of an interior-point filter line-search algorithm for large-scale nonlinear programming. Mathematical Programming 106, 25–57. doi:10.1007/s10107-004-0559-y.

Yamauchi, H., Gumhold, S., Zayer, R., Seidel, H.P., 2005. Mesh segmentation driven by Gaussian curvature. The Visual Computer 21, 659–668. doi:10.1007/s00371-005-0319-x.

Zayer, R., Mlakar, D., Steinberger, M., Seidel, H.P., 2019. Layered fields for natural tessellations on surfaces. ACM Transactions on Graphics 37, 1–15. doi:10.1145/3272127.3275072.

Zhou, K., Synder, J., Guo, B., Shum, H.Y., 2004. Iso-charts: Stretch-driven mesh parameterization using spectral analysis, in: Proceedings of the 2004 Eurographics/ACM SIGGRAPH Symposium on Geometry Processing, Association for Computing Machinery, New York, NY, USA. p. 45–54. doi:10.1145/1057432.1057439.

Zhu, T., Ye, C., Chai, S., Fu, X.M., 2020. Greedy Cut Construction for Parameterizations. Computer Graphics Forum 39, 191–202. doi:10.1111/cgf.13923.